magnetochemistry

MDPI

Article

Effect of Er Substitution on Magnetic and Magnetocaloric Properties of $Nd_{60}Ni_{40}$ Metallic Glass

Nuo Cheng, Song-Tao Yang, Ding Ding and Lei Xia *

State Key Laboratory of Materials for Advanced Nuclear Energy, Shanghai University, Shanghai 200072, China; chengnuo226@shu.edu.cn (N.C.); 24722364yst@shu.edu.cn (S.-T.Y.); d.ding@shu.edu.cn (D.D.)
* Correspondence: xialei@shu.edu.cn; Tel.: +86-136-0186-0721

Abstract

In the present work, we selected an amorphous $Nd_{60}Ni_{40}$ alloy as a basic alloy and added Er with a higher effective magnetic moment and de Gennes factor to replace Nd for the purpose of improving the magnetocaloric performance of the $Nd_{60}Ni_{40}$ amorphous alloy. The formability, magnetization, and magnetocaloric behaviors of the $Nd_{60-x}Er_xNi_{40}$ (x = 5, 10, 15, 20) amorphous alloys were studied. It was found that Er substitution generally improved the glass formability, but simultaneously decreased the Curie temperature, coercivity, and magnetic entropy change peak of the basic alloy. The mechanism for these unexpected results was investigated, and it was supposed that the decreased Curie temperature and the deteriorated magnetocaloric properties may have resulted from the antiferromagnetic coupling between the Nd and Er atoms.

Keywords: metallic glass; magnetic entropy change; Curie temperature; magnetic moment

1. Introduction

Amorphous alloys (AAs), also known as metallic glasses (MG), are a special type of material system that is usually fabricated by rapidly cooling melted alloys to prevent the atoms from arranging into a periodic and ordered structure during solidification [1–3]. The unique atomic configuration of these amorphous materials, that is, long-range atomic disorder and short-range order, not only brings about mechanical advantages such as high strength and hardness, but also demonstrates excellent magnetic properties, including significant magnetocaloric effects (MCEs), outstanding magnetoelastic properties, and so on [4–7].

An MCE refers to an exothermic/endothermic phenomenon due to a change in the magnetic entropy in a magnet upon magnetization/demagnetization. The excellent MCEs in the amorphous alloys make them potential candidate materials for advanced applications in novel magnetic refrigeration solutions that are more efficient and environmentally friendly than the conventional vapor expansion/compression refrigeration technology [8–16]. As the key refrigerant materials, amorphous alloys show several advantages over intermetallic compounds: they present features of a second-order magnetic transition, accompanied by a broadened magnetic entropy change ($-\Delta S_m$) peak, which is much more appropriate for working in an Ericsson cycle. In contrast, intermetallic compounds that exhibit strong magnetocaloric effects (such as $Gd_5(Si,Ge)_4$, $La(Fe,Si)_{13}$, MnFe(P,As), and so on) usually experience a first-order magnetic phase transition and show a sharp but narrow $-\Delta S_m$, which results in a high maximum $-\Delta S_m$ ($-\Delta S_m{}^{peak}$) but low refrigeration capacity ($RC = -\Delta S_m{}^{peak} \times \Delta T_{FWHM}$, where ΔT_{FWHM} is the temperature interval at half of $-\Delta S_m{}^{peak}$);

Check for updates

Academic Editor: Lotfi Bessais

Received: 30 December 2025
Revised: 26 January 2026
Accepted: 3 February 2026
Published: 8 February 2026

Copyright: © 2026 by the authors. Licensee MDPI, Basel, Switzerland. This article is an open access article distributed under the terms and conditions of the Creative Commons Attribution (CC BY) license.

their peak $-\Delta S_m$ temperatures, usually equal to their Curie temperatures (T_c), are tunable, because metallic glasses can be synthesized over a relatively wide range of compositions, and thus, the T_c of these amorphous alloys, depending on their composition, is tailorable. By comparison, the MCEs of intermetallic compounds undergoing a first-order magnetic phase transition are very sensitive to impurities; in other words, the Curie temperatures of these intermetallic compounds are difficult to adjust through micro-alloying or element substitution without dramatically deteriorating their magnetocaloric properties. Thus, the mechanical properties and corrosion resistance of amorphous alloys are better than those of intermetallic compounds [17–19].

Among these MGs, rare-earth (RE) transition metal (TM)-based MGs show great potential as high-performance magnetocaloric materials due to their high magnetic moments brought about by both the RE's 4*f* electrons and the TM's 3*d* electrons. For example, the $-\Delta S_m{}^{peak}$ of Gd-Co-based metallic glasses reaches 10.1 J/(kg × K) under 5 T [20], which is primarily attributed to the substantial magnetic moments of Gd due to its half-filled 4*f* electronic configuration. The $Er_{60}Ni_{30}Co_{10}$ amorphous alloy exhibits a $-\Delta S_m{}^{peak}$ of ~12.1 J/(kg × K) under 5 T [21], and the $Er_{67.5}Co_{32.5}$ binary metallic glass even shows a high $-\Delta S_m{}^{peak}$ of up to 17.47 J/(kg × K) under 5 T [22], both of which are closely related to the high effective magnetic moment of Er (9.58 μ_B). According to the multicomponent rule of metallic glasses, micro-alloying or element substitution may be advantageous for enhancing the glass-forming ability (GFA) of the mother alloys, which makes it easier for them to be fabricated into amorphous refrigerants, and, in addition, may further enhance the MCEs if the proper RE elements are added.

According to our preliminary results, Nd-Ni binary AAs show good GFA and good magnetocaloric performance at low temperatures [23]. In the present work, we considered introducing other earth elements with larger magnetic moments to replace the Nd element for the purpose of improving the GFA and MCE of the Nd-Ni binary MGs. A $Nd_{60}Ni_{40}$ binary MG, with good GFA and magnetocaloric properties, was selected as the basic alloy. Er, with a much higher effective magnetic moment than Nd (3.62 μ_B) and a higher de Gennes factor (G = 2.55 for Er and 1.84 for Nd) [24], was selected as the substitution element. The influences of Er-doping on the GFA, Curie temperature, $-\Delta S_m{}^{peak}$, and RC of the $Nd_{60}Ni_{40}$ MG, and their mechanisms, were investigated.

2. Experimental Methods

Using a high-vacuum furnace under high-purity Ar protection, pure Nd, Er, and Ni metals (purity > 99.9 at%)—mixed simultaneously, pursuant to their respective parts in the composition of $Nd_{60-x}Er_xNi_{40}$ (x = 5, 10, 15, 20)—were arc-melted five times to prepare master alloy ingots. The broken pieces of the master alloy ingots were remelted and subsequently sprayed from a hole at the bottom of the quartz tube onto a high-speed rotating copper roller to prepare thin ribbons. $Nd_{60-x}Er_xNi_{40}$ ribbons with an average thickness of 40 ± 0.5 μm were chosen for the follow-up investigation. XRD analysis using Cu Kα radiation was performed on the $Nd_{60-x}Er_xNi_{40}$ ribbons to ascertain their amorphous structure. A scanning rate of 20 K/min was applied to obtain measurements of their differential scanning calorimetry (DSC) traces on a NETZSCH 404C calorimeter from Germany. The magnetization (M)-temperature (T) curves, the magnetization curves under isothermal conditions (M-H curve), and the hysteresis loops of the MG ribbons were determined by a vibrating sample magnetometer (VSM) module equipped on a Quantum Design 6000 Physical Property Measurement System (PPMS) from Quantum Design, a company based in the United States.

3. Results and Discussion

It was found that none of the $Nd_{60-x}Er_xNi_{40}$ (x = 5, 10, 15, 20) ribbons exhibited obvious sharp crystalline diffraction peaks according to their XRD patterns, as is displayed in Figure 1. Instead, all the samples exhibited smooth diffraction peaks between 30° and 40°, indicating the typical amorphous features of $Nd_{60-x}Er_xNi_{40}$ as-spun ribbons. The amorphous characteristics of the $Nd_{60-x}Er_xNi_{40}$ ribbons were also illustrated by an endothermic glass transition event and sharp exothermic crystallization reaction, as is clearly observed in their respective DSC plots, as shown in Figure 2: (a) x = 5, (b) x = 10, (c) x = 15, and (d) x = 20. The onset temperatures for the glass transition (T_g) and crystallization (T_x) of the MG ribbons, as determined by a tangent method, are summarized in Table 1. The liquidus temperatures (T_l) for the $Nd_{60-x}Er_xNi_{40}$ MG ribbons obtained from the melting curves, as displayed in the inset of Figure 2a–d, are also enumerated in Table 1. Consequently, T_{rg}, defined by D. Turnbull [25], and parameter γ, defined by C. T. Liu and Z. P. Lu [26,27], can be calculated according to

$$T_{rg} = \frac{T_g}{T_l} \quad (1)$$

$$\gamma = \frac{T_x}{T_g + T_l} \quad (2)$$

Table 1. T_g, T_x, T_l, $T_{rg,}$ and γ of the $Nd_{60-x}Er_xNi_{40}$ MG ribbons.

Composition	T_g (K)	T_x (K)	T_l (K)	T_{rg} (K)	γ
$Nd_{55}Er_5Ni_{40}$	427	474	873	0.489	0.364
$Nd_{50}Er_{10}Ni_{40}$	439	482	884	0.497	0.365
$Nd_{45}Er_{15}Ni_{40}$	421	485	888	0.474	0.370
$Nd_{40}Er_{20}Ni_{40}$	433	500	903	0.480	0.374

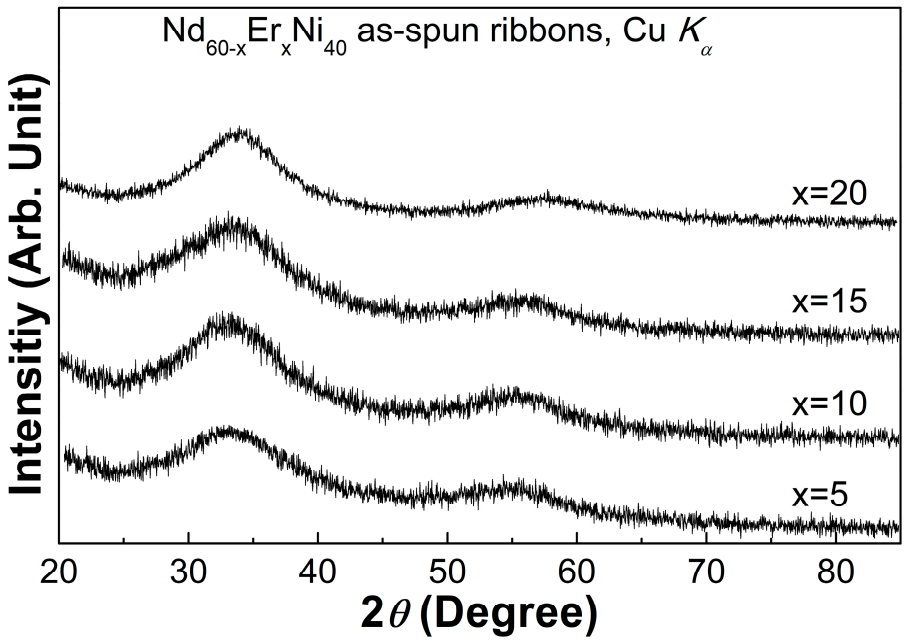


Figure 1. XRD patterns of the $Nd_{60-x}Er_xNi_{40}$ as-spun ribbons.

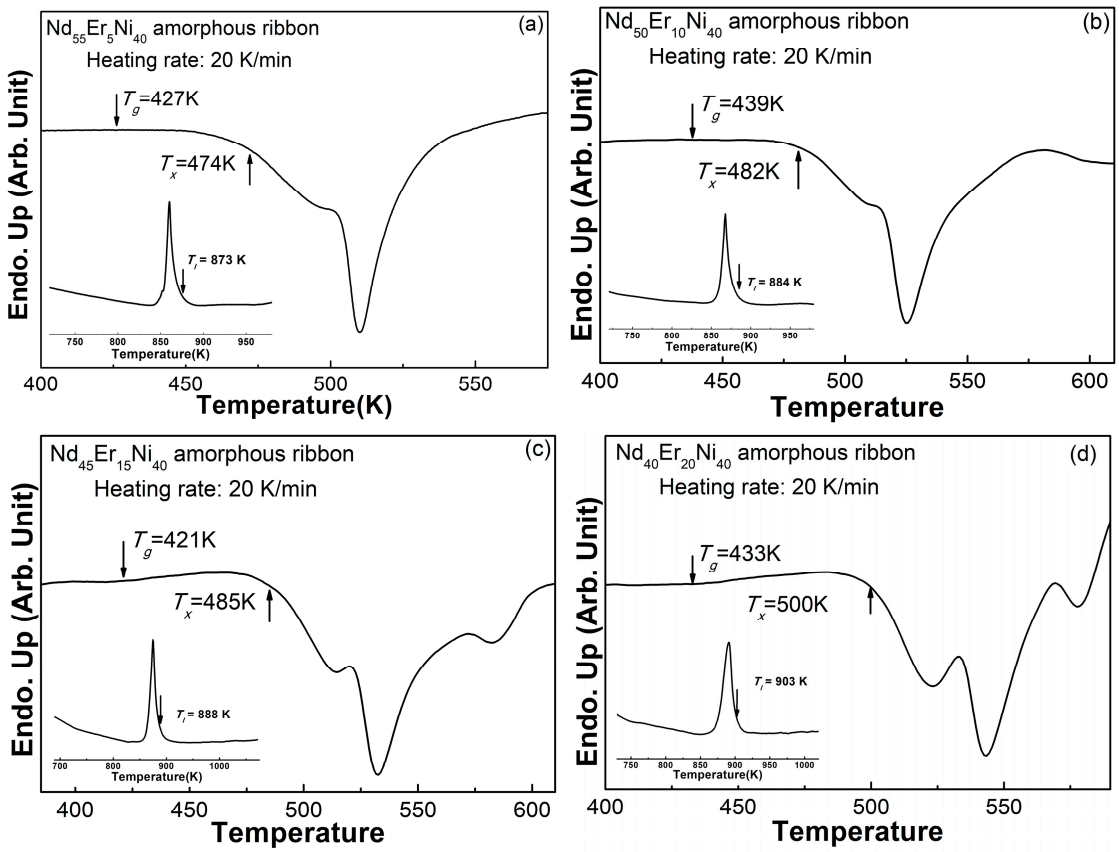


Figure 2. DSC traces of the $Nd_{60-x}Er_xNi_{40}$ amorphous ribbons, (**a**) x = 5, (**b**) x = 10, (**c**) x = 15, and (**d**) x = 20; the insets are their respective melting behaviors.

Figure 3 illustrates the variation in T_{rg} and γ in the $Nd_{60-x}Er_xNi_{40}$ MG ribbons according to their composition. According to the T_{rg} values of the samples, the GFA was enhanced by Er substitution from 5% to 10% and then decreased with any further addition of Er. However, the γ parameter increased monotonously with the addition of Er, indicating the increasing substitution of GFA by Er.

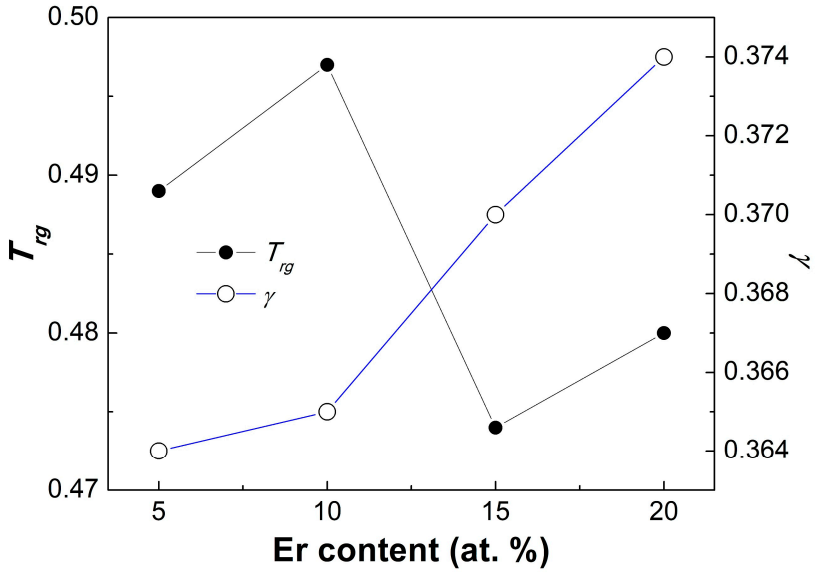


Figure 3. Compositional dependence of T_{rg} and γ in the $Nd_{60-x}Er_xNi_{40}$ MG ribbons.

The *M*-*T* curves of the $Nd_{60-x}Er_xNi_{40}$ MG ribbons were obtained from 5 K to 100 K under an applied magnetic field of 0.03 T, after cooling from ambient temperature to 5 K without a magnetic field (zero field cooling, ZFC), and under a magnetic field of 0.03 T (field cooling, FC). As shown in Figure 4, all the MG ribbons show typical λ-shape characteristics in their field-cooled and zero-field-cooled *M*-*T* curves, indicating the significant spin-glass-like (SGL) behaviors of these MG ribbons. The Curie temperature and the spin-glass-like freezing temperature (T_f) of the $Nd_{60-x}Er_xNi_{40}$ (x = 5, 10, 15, 20) MG ribbons, acquired from their ZFC *M*-*T* curves, are listed in Table 2. The compositional dependence of T_c as well as T_f, as illustrated in Figure 5, indicates that the T_c of the ribbons decreased linearly with the ascending Er content, while the T_f of the $Nd_{60-x}Er_xNi_{40}$ ribbons decreased from x = 5 to x = 10 and then increased with any further addition of Er. The relationship between T_c and Er content was anomalous, because for $Nd_{60-x}Er_xNi_{40}$ MG ribbons with a constant Ni content, T_c maintains a positive proportion relative to the de Gennes factor (*G*) [28] of the ribbons, which can be calculated in a double RE ions system as follows:

$$G = c_1G_1 + c_2G_2 \quad (3)$$

Table 2. T_c, T_f, $-\Delta S_m^{peak}$ and *RC* of the $Nd_{60-x}Er_xNi_{40}$ MG ribbons.

Composition	T_c (K)	T_f (K)	$-\Delta S_m^{peak}$ (J/(kg × K))					*RC* (5T) (J/kg)
			1T	2T	3T	4T	5T	
$Nd_{60}Ni_{40}$	18.3	12.1	2.10	3.89	5.4	6.71	7.86	172
$Nd_{55}Er_5Ni_{40}$	16.6	11.2	1.45	2.77	3.94	5.02	6.08	122
$Nd_{50}Er_{10}Ni_{40}$	15.2	11.4	1.02	2.06	3.17	4.31	5.45	114
$Nd_{45}Er_{15}Ni_{40}$	13.6	11.6	0.59	1.44	2.45	3.55	4.72	109
$Nd_{40}Er_{20}Ni_{40}$	12.8	11.4	0.36	1.12	2.13	2.92	4.45	108

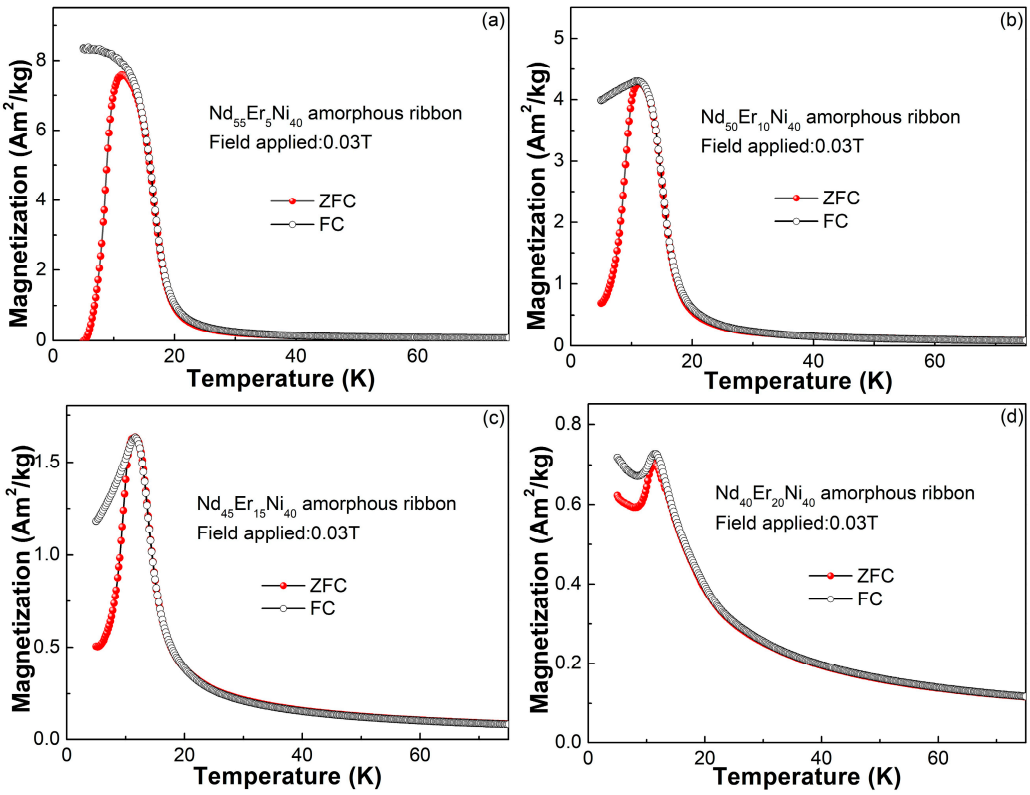


Figure 4. ZFC and FC *M*-*T* curves of the $Nd_{60-x}Er_xNi_{40}$ MG ribbons measured under 0.03 T, (**a**) x = 5, (**b**) x = 10, (**c**) x = 15, and (**d**) x = 20.

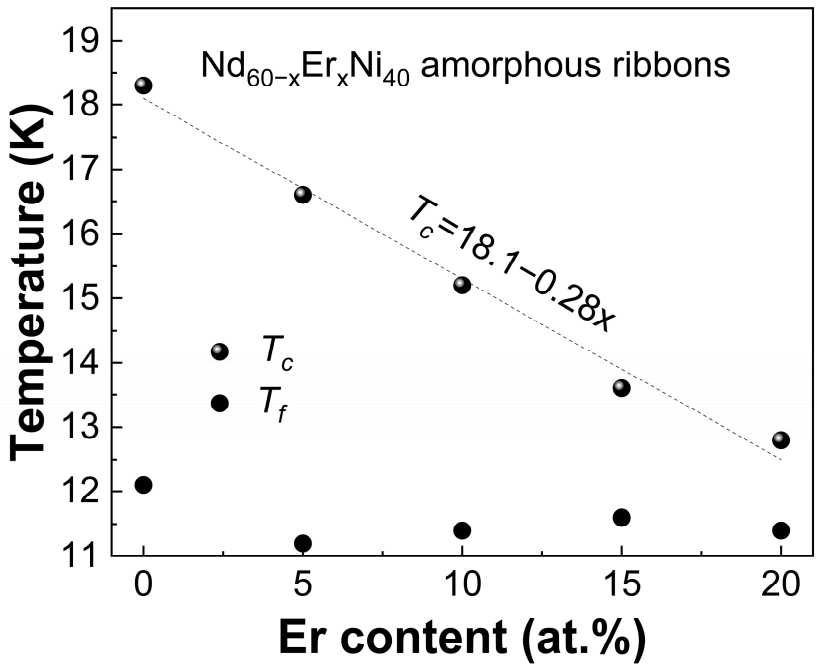


Figure 5. Compositional dependence of T_c and T_f of the $Nd_{60-x}Er_xNi_{40}$ MG ribbons.

Where c_n and G_n are the molar fraction and de Gennes factor of the respective RE ion. As is known, G equals 2.55 for Er and 1.84 for Nd, and thus the increasing substitution of Er for Nd should result in an increasing G in the MGs and give rise to an enhancement of T_c according to Er content, which is obviously the opposite of the experimental results. Considering that the coupling between light RE elements, such as Nd and Ni, is ferromagnetic, while the coupling between heavy RE elements, such as Er and Ni, is antiferromagnetic, the coupling between Nd and Er is most likely antiferromagnetic, according to the Ruderman–Kittel–Kasuya–Yosida (RKKY) indirect exchange model. In the RKKY model, the magnetic moments of localized 4*f* electrons in RE ions are coupled indirectly through the polarization of conduction electrons (primarily 5*d* and 6*s* states) [29–31]. The sign and strength of this exchange depend on the interatomic distances, the Fermi surface topology, and the de Gennes factor G. The de Gennes factor G may be calculated as follows:

$$G = (g_J - 1)^2 J(J+1) \quad (4)$$

where g_J is the Landé g-factor, and J is the total angular momentum quantum number. For light rare-earth elements like Nd ($g_J \approx 0.727$, $(g_J - 1) < 0$), the coupling with transition metals (e.g., Ni 3*d* states) is typically ferromagnetic, leading to a parallel alignment of moments. In contrast, heavy rare-earth elements like Er ($g_J \approx 1.2$, $(g_J - 1) > 0$) exhibit antiferromagnetic coupling with TM moments, resulting in antiparallel alignment. When light and heavy rare-earth elements are mixed, the inter-RE exchange often introduces a competitive antiferromagnetic component arising from the opposing signs of $(g_J - 1)$ and the resulting frustration in the RKKY-mediated interactions [32–34]. This competition disrupts the overall ferromagnetic ordering, effectively reducing the net exchange field and leading to a lower T_c. Furthermore, the antiferromagnetic Nd-Er coupling weakens the total magnetic moment per RE atom, manifesting as reduced magnetization in the *M*-*H* curves and diminished magnetic susceptibility. Consequently, the magnetocaloric effect deteriorates, with $-\Delta S_m{}^{peak}$ and *RC* decreasing due to a lower degree of magnetic entropy change associated with the frustrated spin ordering and enhanced spin-glass-like behavior.

https://doi.org/10.3390/magnetochemistry12020024

To ascertain the above assumptions, the overall system energy of the amorphous $Nd_{55}Er_5Ni_{40}$ alloy was calculated based on a first-principles simulation and compared under two initial configurations: the Nd's magnetic moments being parallel to Er's, and the Nd's magnetic moments being anti-parallel to the Er's. The $Nd_{55}Er_5Ni_{40}$ amorphous structure was first constructed using the stochastic quenching (SQ) method [35–37]. This method commences with an initial structure of 100 atoms distributed in a random way in a cubic cell under a periodic boundary, and is rooted in the single random valley approximation of vibrational transitions (VT) theory. First-principles calculations were performed using the Vienna Ab initio Simulation Package (VASP) [38]. This approach relies on density functional theory (DFT), and the implementation of the projected augmented wave (PAW) pseudopotential [39]. As expected, the simulation results show that the overall energy of the system where the Nd's magnetic moment is antiparallel to the Er's magnetic moment is ~1 meV lower than that of the one where the Nd's magnetic moment is parallel to the Er's magnetic moment, indicating that the atomic magnetic moments between Nd and Er have a stronger propensity to form antiferromagnetic structures. By linearly fitting the T_c plots of the $Nd_{60-x}Er_xNi_{40}$ (x = 0, 5, 10, 15, 20) MG ribbons, the Curie temperature of the samples follows a $T_c = 18.1 - 0.28x$ relationship. The negative slope (-0.28) of the T_c-x relationship may arise from the antiferromagnetic configuration of the atomic magnetic moments between Nd and Er. Supposing that the introduction of Er atoms brings about a negative G value, the total G values of the $Nd_{60-x}Er_xNi_{40}$ MGs will decrease with the addition of Er, which may lead to a decrease in Curie temperature in the MG samples with increasing Er content, and thus, a negative slope of the T_c-x relationship.

The magnetization behaviors of the $Nd_{60-x}Er_xNi_{40}$ MG ribbons are further affected by the SGL phenomena and the competition between ferromagnetic and antiferromagnetic interactions. The isothermal M-H curves of the $Nd_{60-x}Er_xNi_{40}$ ribbons at various temperatures are shown in Figure 6. The M-H curves of the $Nd_{60-x}Er_xNi_{40}$ ribbons clearly exhibit characteristics that are typical of SGL behaviors at temperatures lower than their T_f, and the magnetic susceptibility of the MG samples gradually decreases with increasing Er content. To illustrate the SGL behaviors in a more detailed way, the Arrott plots of the amorphous $Nd_{60-x}Er_xNi_{40}$ ribbons were constructed, as shown in Figure 7a for x = 5, (b) for x = 10, (c) for x = 15, and (d) for x = 20. All the samples show C-shaped Arrott plots with negative slopes below T_f, as shown in the insets of Figure 7a–d, which are the typical SGL characteristics in amorphous samples. On the other hand, the introduction of antiferromagnetic Er atoms may bring about a delay in the magnetic response, resulting in a gradual decrease in magnetic susceptibility with increasing Er content in the Er-doped $Nd_{60}Ni_{40}$ MGs.

The effect of SGL behaviors and the competition between ferromagnetic and antiferromagnetic interactions on the magnetization behaviors of the MG samples may also influence their magnetocaloric performance. Figure 8 shows the magnetic entropy change ($(-\Delta S_m)$-T) curves of the $Nd_{60-x}Er_xNi_{40}$ MG ribbons under applied fields of 1 T, 2 T, 3 T, 4 T, and 5 T. The $-\Delta S_m^{peak}$ of the $Nd_{60-x}Er_xNi_{40}$ MG under various magnetic fields and its RC under 5 T are summarized in Table 2. $-\Delta S_m^{peak}$ under 5 T decreases gradually from 7.86 J/(kg × K) when x = 0, to 6.08 J/(kg × K) when x = 5, 5.45 J/(kg × K) when x = 10, 4.72 J/(kg × K) when x = 15, and 4.45 J/(kg × K) when x = 20. The RC of the $Nd_{60-x}Er_xNi_{40}$ MG ribbons under 5 T also decreases from 172 J/kg (x = 0), to 122 J/kg (x = 5), 114 J/kg (x = 10), 109 J/kg (x = 15), and finally 108 J/kg (x = 20). This suggests that the introduction of Er atoms gives rise to antiferromagnetic coupling in the alloy, subsequently reduces the total magnetic ordering degree, and finally, deteriorates the magnetocaloric properties of the $Nd_{60-x}Er_xNi_{40}$ MGs. As a result, the enhancement of the MCE of RE-TM-based

amorphous alloys not only depends on using RE elements with high magnetic moments, but also on the magnetic coupling between RE elements.

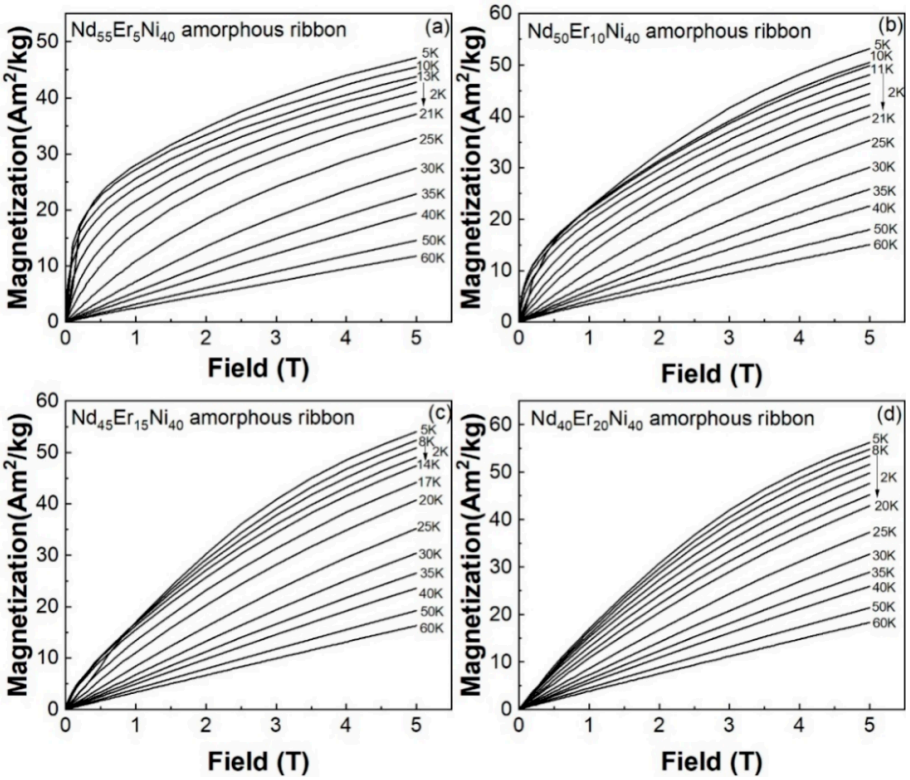


Figure 6. The isothermal *M-H* curves of the $Nd_{60-x}Er_xNi_{40}$ ribbons at various temperatures: (**a**) x = 5, (**b**) x = 10, (**c**) x = 15, and (**d**) x = 20.

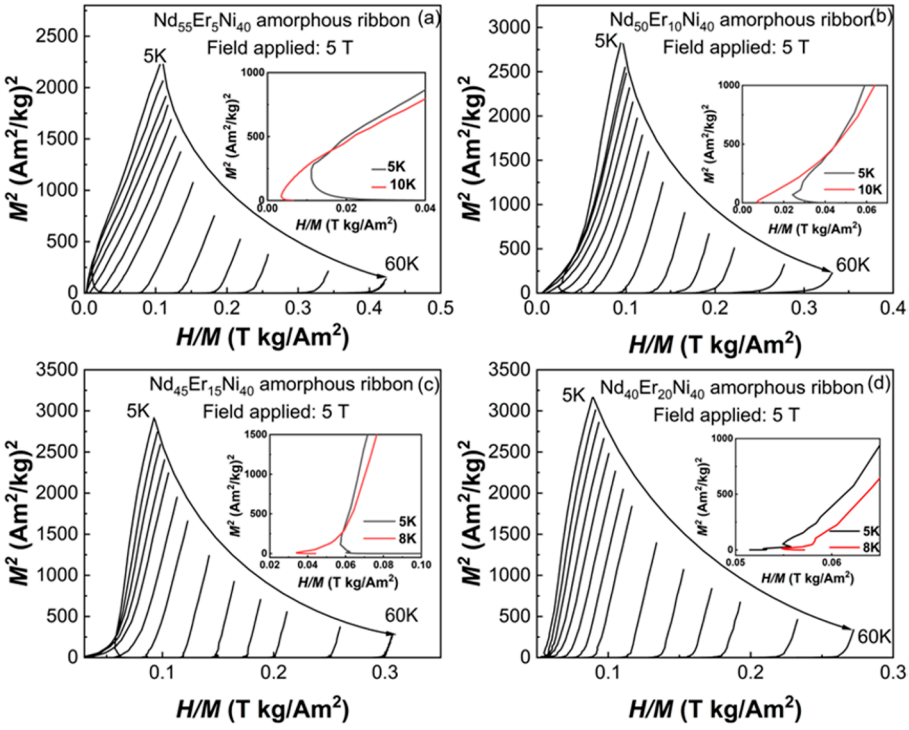


Figure 7. The Arrott plots for the $Nd_{60-x}Er_xNi_{40}$ MGs: (**a**) x = 5, (**b**) x = 10, (**c**) x = 15, and (**d**) x = 20. The insets show the Arrott curves for temperatures below T_f.

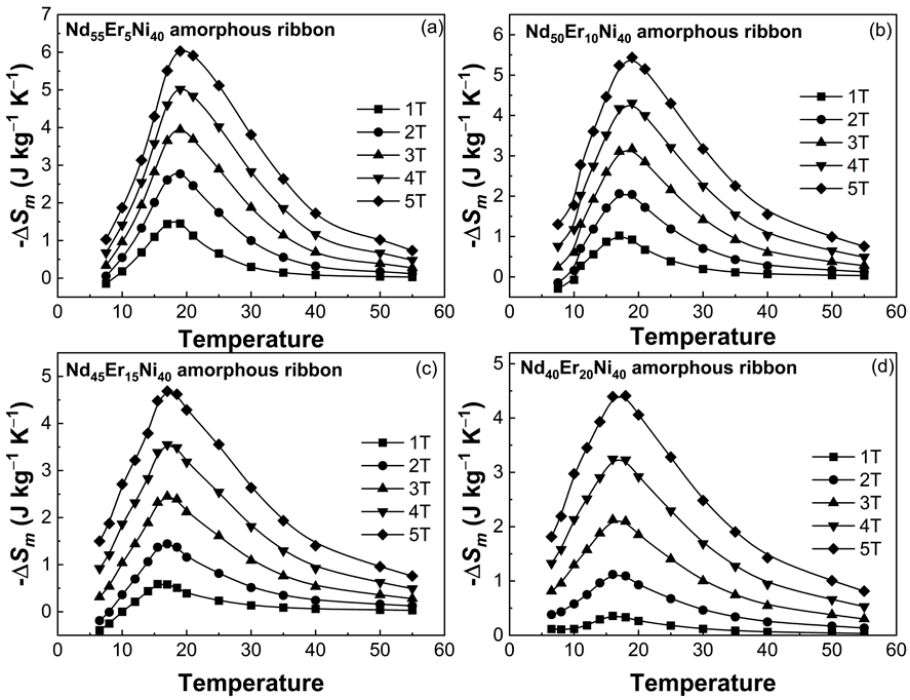


Figure 8. $(-\Delta S_m)$-T curves of the $Nd_{60-x}Er_xNi_{40}$ MGs under 1 T, 2 T, 3 T, 4 T, and 5 T: (**a**) x = 5, (**b**) x = 10, (**c**) x = 15, and (**d**) x = 20.

4. Conclusions

In the present work, we replaced Nd atoms with Er atoms with a higher effective magnetic moment and de Gennes factor, with the hope of improving the GFA and magnetocaloric properties of a $Nd_{60}Ni_{40}$ amorphous alloy. Amorphous $Nd_{60-x}Er_xNi_{40}$ ribbons were successfully fabricated, and their amorphous structure was ascertained by XRD detection. Based on the thermal properties of the $Nd_{60-x}Er_xNi_{40}$ MG ribbons, as measured by DSC, the GFA of these alloys was studied. It was found that the γ parameter increased monotonously with the addition of Er, while T_{rg} v was enhanced by Er substitution from 5% to 10% and then decreased with any further addition of Er, indicating that the Er substitution generally increases the GFA of $Nd_{60}Ni_{40}$ MG. The $Nd_{60-x}Er_xNi_{40}$ MG ribbons show typical SGL behaviors in their M-T curves, and their T_c, as well as T_f, decrease gradually with the addition of Er, although the de Gennes factor of Er is higher than that of Nd. It is supposed that the antiferromagnetic structure of the atomic magnetic moment between Nd and Er brings about a negative G value in Er, resulting in a decrease in total G values in the $Nd_{60-x}Er_xNi_{40}$ MGs with the addition of Er, and finally leads to a decrease in Curie temperature with increasing Er content. On the other hand, Er substitution with a higher effective magnetic moment not only failed to improve the magnetocaloric performance of $Nd_{60}Ni_{40}$ MG, but actually reduced the $-\Delta S_m^{peak}$ and RC of the alloys. It was argued that the introduction of Er atoms gives rise to antiferromagnetic coupling in the alloy, subsequently reducing the total magnetic ordering degree, and finally deteriorating the magnetocaloric properties of the $Nd_{60-x}Er_xNi_{40}$ MGs. Therefore, the enhancement of the MCE of the RE-TM-based amorphous alloy depends not only on the high magnetic moments of the substituted RE elements but also on the magnetic coupling between the RE elements.

Author Contributions: L.X. and D.D. defined the topic and the main content of the review. N.C. and S.-T.Y. jointly completed the experiment. N.C. wrote the initial draft, which was reviewed and completed by L.X. All authors have read and agreed to the published version of the manuscript.

https://doi.org/10.3390/magnetochemistry12020024

Funding: The work was supported by the National Natural Science Foundation of China, grant numbers 51871139 and 52071196.

Institutional Review Board Statement: Not applicable.

Informed Consent Statement: Not applicable.

Data Availability Statement: The original contributions presented in this study are included in the article. Further inquiries can be directed to the corresponding authors.

Conflicts of Interest: The authors declare no conflicts of interest.

References

1. Klement, W.; Willens, R.; Duwez, P. Non-Crystalline Structure in Solidified Gold-Silicon Alloys. *Nature* **1960**, *187*, 869–870. [CrossRef]
2. Wang, W.H.; Dong, C.; Shek, C.H. Bulk Metallic Glasses. *Mater. Sci. Eng. R Rep.* **2004**, *44*, 45–89. [CrossRef]
3. Louzguine-Luzgin, D.V.; Louzguina-Luzgina, L.V.; Churyumov, A.Y. Mechanical Properties and Deformation Behavior of Bulk Metallic Glasses. *Metals* **2013**, *3*, 1–22. [CrossRef]
4. Ming, W.; Guo, X.; Xu, Y.; Zhang, G.; Jiang, Z.; Li, Y.; Li, X. Progress in Non-Traditional Machining of Amorphous Alloys. *Ceram. Int.* **2023**, *49*, 1585–1604. [CrossRef]
5. Zhai, T.G.; Yuan, J.M.; Li, Z.B.; Ding, D.; Xia, L. Magnetocaloric Response of an Eutectic $Er_{69}Ni_{31}$ Amorphous Alloy. *Magnetochemistry* **2025**, *11*, 106. [CrossRef]
6. Li, Z.B.; Yuan, J.M.; Wang, Q.; Ding, D.; Xia, L. Achieving Higher Curie Temperature and Magnetic Entropy Change by Minor Co Substitution for Fe in a $Fe_{88}Pr_{10}Al_2$ Amorphous Alloy. *Intermetallics* **2026**, *189*, 109125. [CrossRef]
7. Yuan, J.M.; Li, Z.B.; Zhai, T.G.; Wang, Q.; Ding, D.; Xia, L. Effect of Pr and Nd Replacement for Zr on the Magnetic and Magnetocaloric Properties of the $Fe_{88}Zr_{10}B_2$ Amorphous Alloy. *Mod. Phys. Lett. B* **2025**, *40*, 2650012. [CrossRef]
8. Franco, V.; Blázquez, J.S.; Ipus, J.J.; Law, J.Y.; Moreno-Ramírez, L.M.; Conde, A. Magnetocaloric Effect: From Materials Research to Refrigeration Devices. *Prog. Mater. Sci.* **2018**, *93*, 112–232. [CrossRef]
9. Gschneidner, K.A., Jr.; Pecharsky, V.K. Magnetocaloric Materials. *Annu. Rev. Mater. Res.* **2000**, *30*, 387–429. [CrossRef]
10. Yu, B.F.; Gao, Q.; Zhang, B.; Meng, X.Z.; Chen, Z. Review on Research of Room Temperature Magnetic Refrigeration. *Int. J. Refrig.* **2003**, *26*, 622–636. [CrossRef]
11. Brown, G.V. Magnetic Heat Pumping Near Room Temperature. *J. Appl. Phys.* **1976**, *47*, 3673–3680. [CrossRef]
12. Hu, F.X.; Shen, B.G.; Sun, J.R.; Cheng, Z.H.; Rao, G.H.; Zhang, X.X. Influence of Negative Lattice Expansion and Metamagnetic Transition on Magnetic Entropy Change in the Compound $LaFe_{11.4}Si_{1.6}$. *Appl. Phys. Lett.* **2001**, *8*, 3675–3677. [CrossRef]
13. Shen, B.G.; Sun, J.R.; Hu, F.X.; Zhang, H.W.; Cheng, Z.H. Recent Progress in Exploring Magnetocaloric Materials. *Adv. Mater.* **2009**, *21*, 4545–4564. [CrossRef]
14. Wada, H.; Morikawa, T.; Taniguchi, K.; Shibata, T.; Yamada, Y.; Akishige, Y. Giant Magnetocaloric Effect of $MnAs_{1-x}Sb_x$ in the Vicinity of First-Order Magnetic Transition. *Phys. B-Condens. Matter* **2003**, *328*, 114–116. [CrossRef]
15. Wang, X.; Wang, Q.; Tang, B.Z.; Yu, P.; Xia, L.; Ding, D. Large Magnetic Entropy Change and Adiabatic Temperature Rise of a Ternary $Gd_{34}Ni_{33}Al_{33}$ Metallic Glass. *J. Rare Earths* **2021**, *39*, 998–1002. [CrossRef]
16. Huo, J.T.; Huo, L.S.; Li, J.W.; Men, H.; Wang, X.M.; Inoue, A.; Chang, C.; Wang, J.Q.; Li, R.W. High-Entropy Bulk Metallic Glasses as Promising Magnetic Refrigerants. *J. Appl. Phys.* **2015**, *117*, 073902. [CrossRef]
17. Inoue, A. Stabilization of Metallic Supercooled Liquid and Bulk Amorphous Alloys. *Acta Mater.* **2000**, *48*, 279–306. [CrossRef]
18. Wang, Q.; Ding, D.; Xia, L. Origin of Random Magnetic Anisotropy in a Fully Amorphous $Tb_{55}Co_{45}$ Alloy. *J. Alloys Compd.* **2025**, *1039*, 183378. [CrossRef]
19. Luo, Q.; Wang, W.H. Magnetocaloric Effect in Rare Earth-Based Bulk Metallic Glasses. *J. Alloys Compd.* **2010**, *495*, 209–216. [CrossRef]
20. Yu, P.; Zhang, N.Z.; Xia, L. Achieving an Enhanced Magneto-Caloric Effect by Melt Spinning a $Gd_{55}Co_{25}Al_{20}$ Bulk Metallic Glass into Amorphous Ribbons. *J. Alloys Compd.* **2016**, *655*, 353–356. [CrossRef]
21. Gao, W.L.; Wang, X.J.; Wang, L.J.; Zhang, Y.K.; Cui, J.Z. Cryogenic Magnetic Properties of $Er_{60}Ni_{30}Co_{10}$ Amorphous Ribbon. *J. Non-Cryst. Solids* **2018**, *484*, 36–39. [CrossRef]
22. Wang, P.; Wang, Q.; Yuan, J.; Zhai, T.; Li, Z.; Ding, D.; Xia, L. Excellent Magnetocaloric Effect Near the Hydrogen Liquefaction Temperature of a Binary $Er_{67.5}Co_{32.5}$ Metallic Glass. *J. Non-Cryst. Solids* **2024**, *646*, 123224. [CrossRef]
23. Zhang, H.T.; Wang, Q.; Xia, L. Investigation on the Glass Forming Ability, Magnetic Properties of Nd-Ni Binary Metallic Glasses and the Mechanism Involved. *J. Alloys Compd.* **2025**, *1027*, 180569. [CrossRef]
24. Coey, J.M.D. *Magnetism and Magnetic Materials*, 1st ed.; Cambridge University Press: Cambridge, UK, 2010. [CrossRef]
25. Turnbull, D. Under What Conditions Can a Glass Be Formed? *Contemp. Phys.* **1969**, *10*, 473–488. [CrossRef]

26. Lu, Z.P.; Liu, C.T. Glass Formation Criterion for Various Glass-Forming Systems. *Phys. Rev. Lett.* **2003**, *91*, 115505. [CrossRef]
27. Lu, Z.P.; Liu, C.T. A New Glass-Forming Ability Criterion for Bulk Metallic Glasses. *Acta Mater.* **2002**, *50*, 3501–3512. [CrossRef]
28. Jensen, J.; Mackintosh, A.R. *Rare Earth Magnetism: Structures and Excitations*, 1st ed.; Oxford University Press: Oxford, UK, 1991. [CrossRef]
29. Ruderman, M.A.; Kittel, C. Indirect Exchange Coupling of Nuclear Magnetic Moments by Conduction Electrons. *Phys. Rev.* **1954**, *96*, 99–102. [CrossRef]
30. Kasuya, T. A Theory of Metallic Ferro- and Antiferromagnetism on Zener's Model. *Prog. Theor. Phys.* **1956**, *16*, 45–57. [CrossRef]
31. Yosida, K. Magnetic Properties of Cu-Mn Alloys. *Phys. Rev.* **1957**, *106*, 893–898. [CrossRef]
32. Hindmarch, A.T.; Hickey, B.J. Direct Experimental Evidence for the Ruderman-Kittel-Kasuya-Yosida Interaction in Rare-Earth Metals. *Phys. Rev. Lett.* **2003**, *91*, 116601. [CrossRef] [PubMed]
33. Blanco-Rey, M.; Castrillo, R.; Ali, K.; Gargiani, P.; Ilyn, M.; Gastaldo, M.; Paradinas, M.; Valbuena, M.A.; Mugarza, A.; Ortega, J.E.; et al. The Role of Rare-Earth Atoms in the Anisotropy and Antiferromagnetic Exchange Coupling at a Hybrid Metal–Organic Interface. *Small* **2024**, *20*, 2402328. [CrossRef]
34. Swift, W.M.; Wallace, W.E. Reversal of Coupling in Intermetallic Compounds Containing Two Rare Earth Elements. *J. Solid State Chem.* **1971**, *3*, 180–183. [CrossRef]
35. Holmström, E.; Bock, N.; Peery, T.; Chisolm, E.; Lizárraga, R.; De Lorenzi-Venneri, G.; Wallace, D. Structure Discovery for Metallic Glasses Using Stochastic Quenching. *Phys. Rev. B* **2010**, *82*, 024203. [CrossRef]
36. De Lorenzi-Venneri, G.; Wallace, D.C. Single-Random-Valley Approximation in Vibration-Transit Theory of Liquid Dynamics. *Phys. Rev. E* **2007**, *76*, 041203. [CrossRef]
37. Lizárraga, R. Structural and Magnetic Properties of the Gd-Based Bulk Metallic Glasses $GdFe_2$, $GdCo_2$, and $GdNi_2$ from First Principles. *Phys. Rev. B* **2016**, *94*, 174201. [CrossRef]
38. Kresse, G.; Furthmüller, J. Efficient Iterative Schemes for Ab Initio Total-Energy Calculations Using a Plane-Wave Basis Set. *Phys. Rev. B* **1996**, *54*, 11169–11186. [CrossRef] [PubMed]
39. Blöchl, P.E. Projector Augmented-Wave Method. *Phys. Rev. B* **1994**, *50*, 17953. [CrossRef]

Disclaimer/Publisher's Note: The statements, opinions and data contained in all publications are solely those of the individual author(s) and contributor(s) and not of MDPI and/or the editor(s). MDPI and/or the editor(s) disclaim responsibility for any injury to people or property resulting from any ideas, methods, instructions or products referred to in the content.